Check for updates

Synchronization modes of chitosan surfers with various sizes

Bálint Gárdi,[†][a] Pawan Kumar,[†][ab] Dezső Horváth [ID][c] and Ágota Tóth [ID][*a]

Transition from partial to complete synchrony is generally governed in coupled oscillator networks by systematic tuning of the coupling strength. In active matter systems, however, such controlled progression is far more elusive, owing to the intrinsically weaker interactions and erratic motility of particles. Here, we investigate the collective dynamics of three and four chitosan motors at the air–liquid interface, where the effective coupling emerges from the competition between capillary attraction and Marangoni-driven repulsion. By tuning the bead size, we modulate the coupling strength and thereby the synchronization modes. For quasi-identical beads, chitosan beads exhibit collective synchrony with breathing-like behavior, whereas size asymmetry gives rise to partial synchrony. In the four-bead configuration, sensitivity to initial conditions leads to markedly different macroscopic trajectories, including switching between synchronization states. The temporal evolution of inter-beads distance and synchronization phases quantitatively confirms these transitions.

1 Introduction

Active constituents effectively harness environmental energy to generate self-propulsion on micro to macro scales.[1] This phenomenon is crucial for the migration and survival of living organisms, allowing them to navigate complex environments and adapt to dynamic ecological niches. Beyond individual motility, these behaviors become particularly compelling when viewed through the framework of collective behavior. Localized interactions between individuals, often mediated by environmental cues, can spontaneously generate highly organized emergent group dynamics, ranging from the collective oscillations of cells[2] to swarming behavior in animals.[3] Inspired by these natural paradigms, researchers have developed various artificial motors that guide mimic such autonomous activities and cooperative behaviors. These include artificial swimmers, capable of propulsion in liquid phases, and artificial surfers, which propel at air–liquid interfaces.

The motility of artificial particles arises from the spontaneous breaking of symmetry in their surrounding environments driven by mechanisms such as the Marangoni effect,[4,5] bubble generation,[6,7] and self-phoresis.[8] Among these, the Marangoni effect, where surface tension gradients drive autonomous motion, has emerged

as a common mechanism for active surfer particles. Over the years, numerous experimental and theoretical investigations have reported intriguing behaviors exhibited by isolated surfers, such as oscillatory motion,[9–13] rotational motion,[14,15] filament-like undulations,[16] spontaneous splitting[17–20] and pathway selection.[21,22] Although significant studies have focused on liquid droplets and solid objects. Recent advances have also demonstrated that sol–gel transitions *in situ* under non-equilibrium conditions can program the self-propulsion of polysaccharide polymer droplets, allowing for a range of dynamic activities through controlled mass flux and polymer composition.[23,24]

In multibody systems, the emergence of collective behaviors among artificial surfers is dictated by nonlinear physicochemical interactions. These interactions arise from the interplay of interfacial forces, chemical and flow-field distributions in the vicinity of individual components. Typically, the localized distribution of chemical fields and the outflow of the components around individual Marangoni surfers result in repulsive forces because in the confined space between the particles the lowering of surface tension is greater than on the opposite side. Hence, the intersection of these concentration fields repels neighboring surfers and facilitates the emergence of ordered lattice-like arrangements of camphor boats.[25] The influence of confined geometry and constraints leads to distinct synchronized behaviors in camphor boats,[26,27] filaments,[28] ribbons,[29,30] and active droplets.[31] Conversely, the attractive forces, driven by buoyancy and surface deformations at the air–liquid interface, promote aggregations of catalytic tubes.[32] The antagonistic interplay of attractive and repulsive interactions underpins the wide variety of patterns and dynamics, including spatial patterning in the

[a] *Department of Physical Chemistry and Materials Science, University of Szeged, Rerrich Béla tér 1., Szeged, H-6720, Hungary. E-mail: atoth@chem.u-szeged.hu*

[b] *Department of Chemical Engineering, Indian Institute of Technology Kanpur, Kanpur (UP) 208016, India*

[c] *Department of Applied and Environmental Chemistry, University of Szeged, Rerrich Béla tér 1., Szeged, H-6720, Hungary*

[†] These authors contributed equally to this work.

surfactant droplet assembly,[33] predator–prey dynamics,[34] quorum sensing–like behavior,[35] atomic-like behavior,[36,37] dynamic clustering,[38,39] and collective oscillations in synchrony.[40]

However, most studies of collective behavior are focused on interactions among quasi-identical particles. The role of heterogeneity in particle sizes and activity is expected to influence their coupling strength, which can generate new forms of patterns. Recent work by Roy *et al.*[41] has demonstrated that the interactions of mismatched volumes of pair droplets exhibit the transition from in-phase to anti-phase synchronization. Despite these advances, collective behavior in systems with surfers of different sizes remains scarcely studied.

In this study, we investigated the collective dynamics of three and four chitosan motors with varying size distributions at the air–liquid interface. By varying the size of the beads, we tuned both attractive and repulsive interactions between the motors. We observed the collective oscillations in beads of nearly identical size. In addition, we identified distinct patterns of partial synchronization and frustration behavior in asymmetric size configurations of the beads.

2 Experimental

2.1 Solution preparation

Chitosan was adequately homogenized in an aqueous acetic acid solution with $c = 1.0$ mol dm^{-3}. The gelation process, which induces the formation of the movement patterns, is driven by an acid–base reaction in an aqueous environment. Therefore, double-purified deionized water was used to prepare the required mixtures. In a 1 : 4 volume ratio acetic acid-water mixture, 0.0750 g of medium molecular weight chitosan and 0.3717 g of GdCl$_3$·6H$_2$O was added. To facilitate the evaluation of the measurements, a small amount of solid methylene blue dye was added to the sols. To achieve homogeneity of the sol,[23] the solid polysaccharide was slowly stirred in the acidic mixture for 24 hours using a magnetic stirrer in a closed system. The subsequent rest period in a cool environment (4 °C) for a few hours allowed the proper polymer structure to develop. The positively charged long-chain molecules formed complexes with the negatively charged acetate ions, resulting in a more viscous chitosan sol ($\eta = 46$ mPa s at 25 °C). To the prepared chitosan sol, 1.60 ml of absolute ethanol was added and the mixture was stirred for another two hours. The ethanol-containing sol was then stored in a properly sealed container in a cool place for one day until use.

The gel-state beads formed from the ethanol-containing sol were referred to as active particles, while those formed without ethanol were called inactive particles. In the experiments, sols containing chitosan were added to an alkaline NaOH solution with a given volume and a concentration of 3.00 mol dm^{-3}.

2.2 Experimental setup and evaluation procedure

The dynamics of the beads had been studied in a 13.5 cm diameter plexiglass Petri dish and a 6.5 cm diameter glass Petri dish at 24 ± 1 °C. The smaller dish contained 17 cm^3, while the larger one held 110 cm^3 of a 3.00 M sodium hydroxide solution.

From the sol with the desired composition, a peristaltic pump was used to disperse a similar amount of polymer into the NaOH-containing Petri dishes for the various measurements. The pump was set at a constant flow rate required to produce particles of a specific size. A 0.51 mm inner diameter medical injection needle was attached to the pump, where the accumulating liquid eventually formed a droplet, which detached and fell into the alkaline solution. The aminopolysaccharide chains were cross-linked by an acid–base reaction with hydroxide ions, resulting in deformed boat-shaped hydrogel particles or beads. Beads with two different sizes were generated reproducibly: The small droplets (2–3 mm in diameter) detached from the tip of the injection needle at a flow rate of 0.2 rpm, while the large droplets (4–5 mm in diameter) from the end of a plastic casing (1.16 mm inner diameter) fit onto the injection needle at a flow rate of 1.2 rpm. For each set of arrangement, the experiments were repeated at least five to seven times.

The experiments were recorded with a GoPro camera mounted on a stand and positioned 12.5 cm from the stage. The motion of the beads was determined from the images by in-house software. The file generated by the program contained the image sequence numbers along with the corresponding parameters for each bead: the area of the red-marked circle found using the global maximum search function, the area of the blue-drawn circle fitted to the detected points, the x- and y-coordinates of the center of the circle, and the radius calculated from the fitted circle. At each time, the distance between the individual beads was determined from the x- and y-coordinates of the bead centers using the following equation:

$$d_{i,j} = \sqrt{\left(x_i - x_j\right)^2 + \left(y_i - y_j\right)^2}, \qquad (1)$$

where i and j denote the beads' number whose distance was calculated. To illustrate synchronization, the distances between particles were plotted as a function of time. Then, to quantitatively characterize the periodic motion, the period was calculated from the local maxima of the inter-bead distances. To quantify the synchronization, cross-correlation, phase locking values, and mean coherence were determined with an in-house Python script.

3 Results and discussion

Once formed upon contact, the gel beads exhibit self-propelled motion and meander independently on the entire liquid surface as discussed in ref. 23. This period, characterized by constant motion, later evolves into the stop-and-run phase because of the decrease in the ethanol content. At this stage, the lowering of surface tension around the individual beads is not sufficient for self-propulsion; they begin to form clusters due to capillary attraction. In the clustering stage, the entire group exhibits a slow motion, mainly driven by the bulk fluid flow, remnant of the initial stage. More interesting is the

motion within the cluster on a shorter time scale, controlled by attractive and repulsive forces and this is what we explore here. The close-packed cluster, shown as a grayscale image in Fig. S1(a), for multiple beads without ethanol supports the presence of capillary attraction among them. To examine the effect of ethanol release from the beads, we added ethanol (without the gadolinium salt) to the polymer. In this case, the chitosan beads do not develop any air–liquid interface deformations[40] and exhibit self-propulsion in an unsynchronized manner (see Fig. S1(b) in SI). Finally, the beads come to rest while remaining spatially separated by a characteristic interparticle distance, indicating the effect of Marangoni repulsion (see Fig. S1(c) in SI).

3.1 Collective behavior of three active beads

First, we studied the interactions of three quasi-identical beads of small size (2.91 mm diameter). To identify the motion of individual beads, each bead is represented by a number, as indicated in the grayscale image in Fig. 1.

After forming the cluster, all particles oscillate with a maximum inter-particle distance of about 0.2 mm. The local maxima and minima of the distances between the particles coincide, as shown in Fig. 1, corresponding to the so-called breathing motion, that is, the three particles move away from each other and towards each other simultaneously with a period of 0.20 ± 0.04 s. In-phase synchronization is also proven in Fig. 2 which illustrates that within 10 s approximately 50 cycles take place and the phases of the distances between different beads coincide as depicted in the inset figure. In Fig. 2 the number of cycles is obtained by locating each maximum in the inter-particle distance. From these maxima, a phase value (φ) can be assigned to each measured data point according to

$$\varphi = 2\pi \frac{t - t_{m,i}}{t_{m,i+1} - t_{m,i}}, \qquad (2)$$

where $t_{m,i}$ and $t_{m,i+1}$ represent the maximum separation before and after time t, respectively, i.e. $t_{m,i} \le t \le t_{m,i+1}$. This is presented in the inset. The phase angle of the corresponding inter-particle
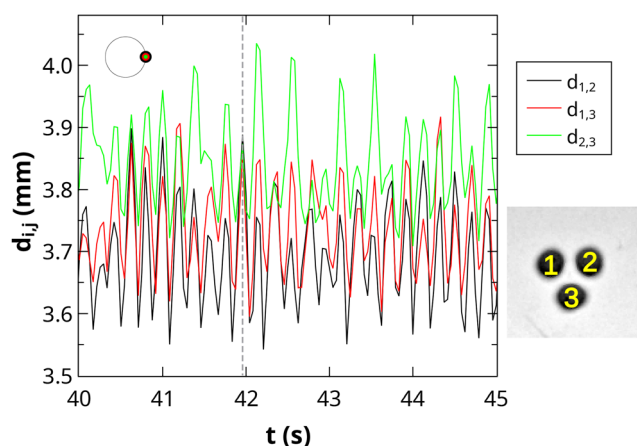

Fig. 1 Dynamics of three small motors: distance between beads i and j ($d_{i,j}$) as a function of time. Phases of oscillation at $t = 42$ s indicated by vertical dashed line shown in the inset in a small circle along with the corresponding top view of the beads with field view of 13 mm × 13 mm.

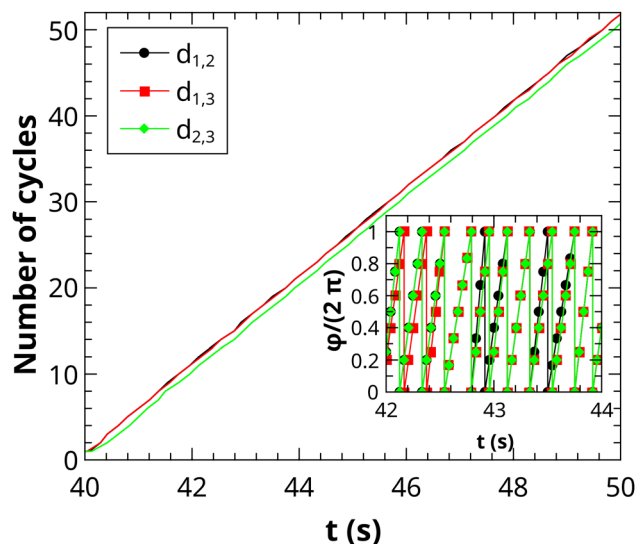

Fig. 2 Dynamics of three small motors: temporal evolution of the number of cycles for the distances between beads i and j ($d_{i,j}$) with the corresponding phases of oscillation shown in the inset figure.

separations at selected times is also presented by small circles in the figures as the angle of rotation with respect to the x-axis.

This synchronized behavior of beads with phase locking values ≥ 0.9999 and mean coherence of 1.0, and heat map of maximum cross-correlations in Fig. S2 in SI is in excellent agreement with our earlier findings,[40] where we attributed such collective phenomena to the interplay between capillary-driven attractions and ethanol-mediated repulsive forces.

An increase in the size of the beads has a multiple effect on the interaction between them. A larger bead creates a larger depression on the liquid surface, resulting in greater capillary attraction, i.e., greater coupling strength (see Table S1 in SI). It also affects the time scale as a larger bead experiences a greater viscous drag that tends to slow it down. However, the larger bead contains more ethanol, therefore, its diffusion can provide fuel longer to lower surface tension that can drive repulsion, the counteracting force. To study these size effects, we investigated the dynamics of the system where the size of one bead is increased by 70% to 4.25 mm, while the others are kept small (2.45 mm). A continuous approaching-retreating motion developed between the two smaller particles, which is shown in Fig. 3 as oscillations between beads 1 and 2 with a period of 0.32 ± 0.04 s (cf. Movie S1 in SI). The capillary attraction between the large and small beads is strong, so the small ones oscillate around the big one at an almost constant distance.

If we increase the size of one more bead, we observe another form of movement (see movie S2 in SI). In the experiment shown, the bead sizes are 4.45 mm (1, 2) and 3.24 mm (3), as numbered in the grayscale image of Fig. 4.

No oscillation occurred between the two nearly identical, larger beads, as seen in the smaller amplitude (0.08–0.06 mm) of the black solid curve around 5.68 mm in Fig. 4. The smaller bead performed a dynamic, continuous back-and-forth motion between the two larger particles, which can be observed in the
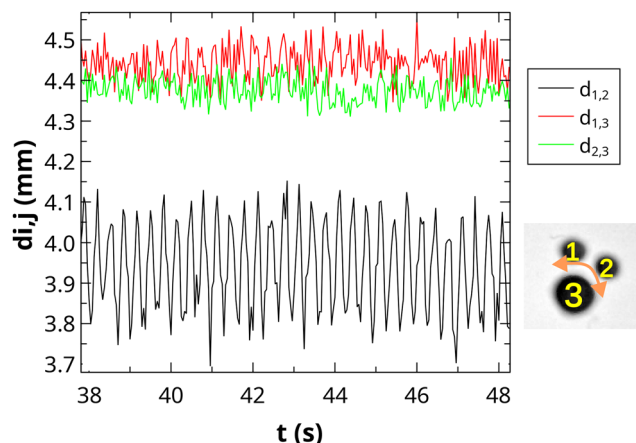
Fig. 3 Breathing dynamics of one big and two small motors: distance between beads i and j ($d_{i,j}$) as a function of time. Top view of beads with field of view of 12 mm × 11 mm.

~0.2 mm amplitude changes of the solid green and red curves in Fig. 4. The repulsion between the beads pushes the smaller particle out of the neighborhood of the larger ones, but the attractive force pulls it back to its original position. The temporal stability of the in-phase synchronization is also characterized by a constant period of 0.31 ± 0.04 s in the time frame shown.

Finally, we investigated the collective behavior of three large beads, approximately 6.5 mm in size (see Movie S3 in SI). Fig. 5 illustrates a similar in-phase synchronization to that depicted in Fig. 1 with a slightly longer period of 0.29 ± 0.04 s. The increase in the time period of their back-and-forth rhythmic activity involving larger beads is expected to be affected by the drag force.

The heat maps of maximum cross-correlations in Fig. S2 in SI show that the complete synchronization seen for three small beads is retained for the big beads.
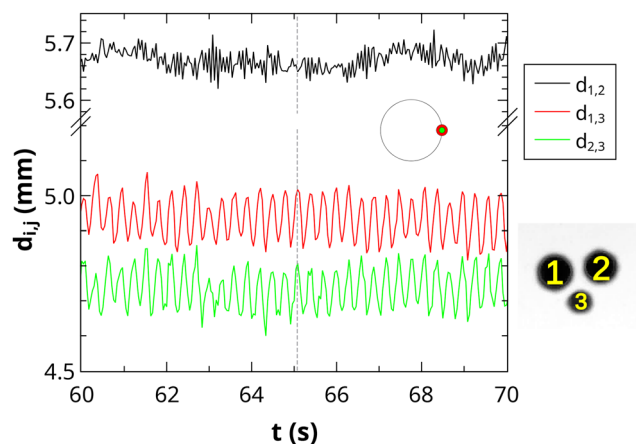

Fig. 4 Dynamics of one small and two big motors: distance between beads i and j ($d_{i,j}$) as a function of time. Phases of oscillation at $t = 65$ s indicated by vertical dashed line shown in the inset in a small circle along with the corresponding top view of the beads with field view of 15 mm × 13 mm.
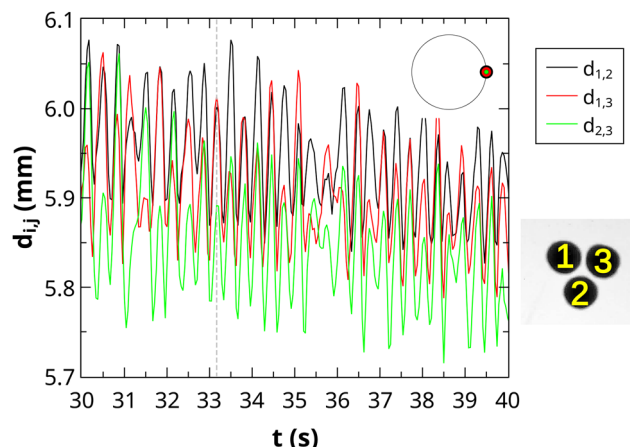

Fig. 5 Dynamics of three big motors: distance between beads i and j ($d_{i,j}$) as a function of time. Phases of oscillation at $t = 33.2$ s indicated by vertical dashed line shown in the inset in a small circle along with the corresponding top view of the beads with field view of 18 mm × 16 mm.

3.2 Collective behavior of four active beads

First, we have investigated the synchronized motion between four chitosan beads of the same small size (~2.60 mm). After forming the square-shaped cluster as shown in the grayscale image in Fig. 6, all beads oscillate periodically with a time period of 0.38 ± 0.02 s in full synchrony (see heat map of maximum cross-correlations in Fig. S3 in SI) and exhibit breathing motion similar to that in Fig. 1, producing a final equidistant assembly as the equilibrium state. When cluster formation occurs at a later stage, significant depletion of ethanol affects the activity of the beads. This change in the local environmental conditions influences the clustering patterns of the beads following collisions, as the altered conditions can prevent them from organizing into favorable square configurations. Instead, beads tend to assemble in atypical patterns, as illustrated in the grayscale image in Fig. 7, suggesting that the timing of the cluster formation critically influences the resulting assembly.
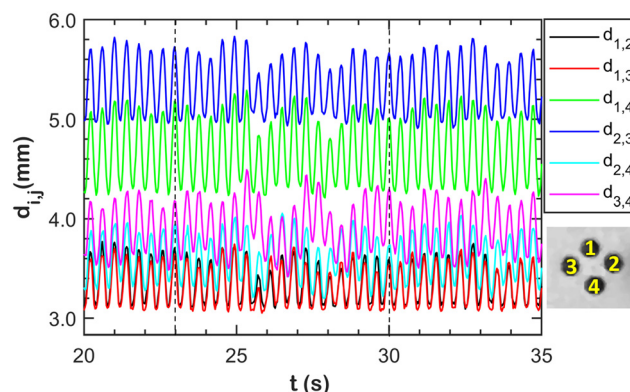

Fig. 6 Dynamics of four small motors: distance between beads i and j ($d_{i,j}$) as a function of time. The dashed lines at $t = 23$ s and 30 s indicate that the oscillations of the beads are in phase. Field of view of grayscale image is 11 mm × 10 mm.
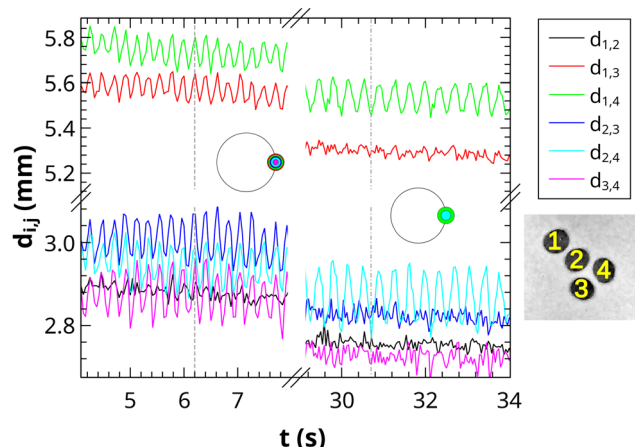
Fig. 7 Dynamics of four small motors: distance between beads i and j ($d_{i,j}$) as a function of time. Phases of oscillation at $t = 6.2$ s indicated by vertical dashed line shown in the inset in a small circle along with the corresponding top view of the beads (field view: 12 mm × 11 mm) and at $t = 30.7$ s indicated by vertical dashed dotted line.

Fig. 8 Dynamics of two small and two big motors with translational motion: distance between beads i and j ($d_{i,j}$) as a function of time. Phases of oscillation at $t = 35.5$ s indicated by vertical dashed line shown in the inset in a small circle along with the corresponding top view of the beads (field view: 12 mm × 11 mm).

The unusual cluster developed exhibits small-amplitude oscillations, where beads 1 and 4 are synchronized through bead 2. The distance between beads 2 and 4, shown by the solid cyan curve, is smaller than the distance between beads 1 and 4 due to the proximity of the beads, resulting in oscillations with an amplitude of ~0.1 mm and a period of 0.36 ± 0.04 s. The period of oscillations between beads 1 and 4 is the same within the experimental error, and the amplitude is also similar. The two periodic behaviors indicate a synchronized behavior with the same phase, which occurs at the green turning part of the trajectory in Fig. 7 and does not significantly affect the motion of the four particles. The heat maps in Fig. S4 in SI, however, reveal that the change in motion pattern results in partial synchrony only.

We have also investigated the appearance of new behaviors in systems consisting of four self-propelled chitosan motors arising from the size changes. When two smaller and two larger chitosan beads form clusters, depending on the initial conditions, a different behavior is observed. The in-phase synchronized oscillations are embedded in translational motion (*cf.* trajectory in Fig. S9 in SI), where the larger beads (beads 1 and 2) had diameters of 4.29 mm, while the smaller ones (beads 3 and 4) had 3.05 mm.

Due to their size, oscillations between large beads are negligible, as indicated by the almost constant distance between them (black solid line) in Fig. 8. The temporal evolution of their inter-particle distance is distinct from the rest, as shown by the heat map of Fig. S5 in SI. However, a significant oscillation with a 0.5–0.7 mm amplitude and a period of 0.42 ± 0.04 s occurs between the two small beads, as shown by the magenta curve. This spatial and temporal periodic motion also affects the further interactions: oscillation with the same periodicity occurs between beads 1 and 3 (red line) and between beads 2 and 4 (cyan line). This partially synchronized behavior, where only smaller beads are synchronized, and ejection-retraction is formed by a pair of beads of different sizes, was also observed in the three-bead system (see Fig. 3).
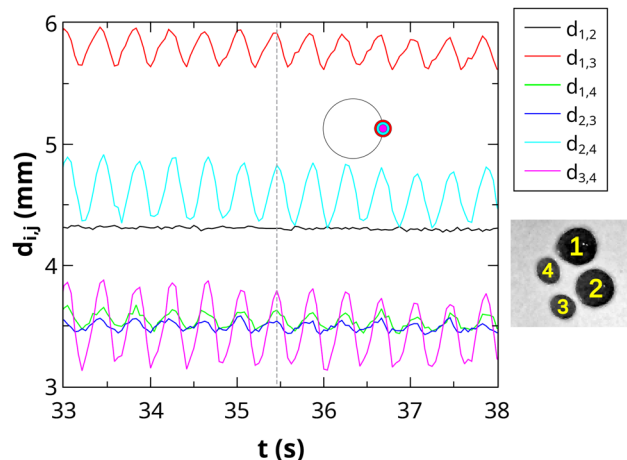
Changing the initial conditions slightly by increasing the diameters of the larger beads to ~3.70 mm, while keeping the smaller ones at ~2.18 mm, as shown in Fig. 9, leads to a different form of collective behavior. Unlike the previously observed case (Fig. 8), where the cluster exhibited translational motion, the present configuration gives rise to rotational motion of the assembly, as illustrated by the representative x–y trajectories in Fig. S10 in SI. During this rotational motion, a switching in the synchronized behavior is observed. Similarly to the earlier scenario (Fig. 8), the larger beads (labeled as 2 and 3 in the grayscale image in Fig. 9) do not oscillate, resulting in constant inter-droplet distances over time (see the blue curve in Fig. 9). In the first stage (around 100 to 110 s), the distances
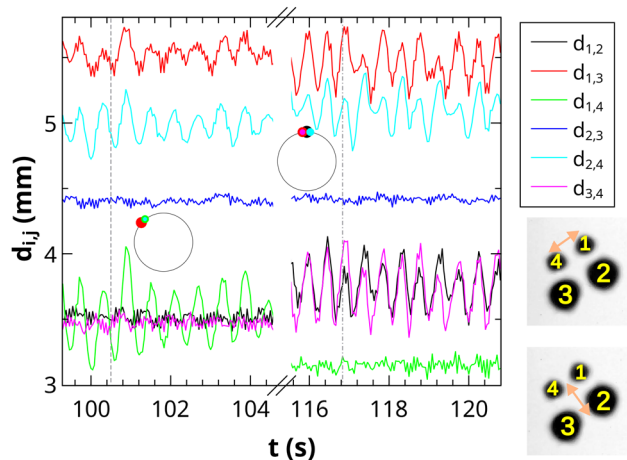

Fig. 9 Dynamics of two small and two big motors with rotational motion: distance between beads i and j ($d_{i,j}$) as a function of time. Phases of oscillation at $t = 100.5$ s indicated by vertical dashed line shown in the inset in a small circle along with the corresponding top view of the beads and at $t = 117$ s indicated by vertical dashed dotted line (field view: 11 mm × 11 mm).

between diagonally placed pair of beads of different sizes, namely (1,3) and (2,4), as well as between the smaller beads (1,4), vary periodically with a period of 0.52 ± 0.04 s. In contrast, the distances between the pair of beads (1,2) and (3,4) remain constant, as shown by the black and magenta time series in Fig. 9. This dynamic state corresponds to oscillations of the smaller beads 1 and 4, which move in and out (as indicated by the arrow in the grayscale image), while remaining in contact with the larger beads 2 and 3.

Furthermore, the activities of the beads switch to a new dynamic state, as indicated by the temporal evolution of their pairwise distances $d_{i,j}$ after approximately 115 s in Fig. 9. The gradual decay in the amplitude of $d_{i,j}$ for the oscillating beads demonstrates that this new state emerges progressively, most likely influenced by the depletion of ethanol. In this regime, the distance between the smaller beads 1 and 4 (green line) reaches a steady state, while the asymmetric bead pairs (3,4) and (1,2) begin to oscillate periodically with a period of 0.47 ± 0.04 s, as shown by the corresponding magenta and black curves. The phases of these oscillations coincide, indicating that the cluster attains a phase-synchronized state (see Fig. S11 in SI), which is also apparent on the heat maps of maximum cross-correlations in Fig. S6 in SI.

To further investigate the influence of bead size, we examined a system consisting of three larger chitosan beads with diameters of ∼3.55 mm and one smaller bead with a diameter of ∼2.26 mm, as shown in the grayscale images of Fig. 10. No significant oscillations are observed between the larger beads (*i.e.*, between motors 2 and 3, and between motors 3 and 4), as indicated by the nearly constant lines of $d_{2,3}$ and $d_{3,4}$. In contrast, the separation between the larger beads placed diagonally (motors 2 and 4, $d_{2,4}$) initially shows small-amplitude oscillations (cyan line), which after approximately 158 s, increase in amplitude and result in a longer oscillation period.
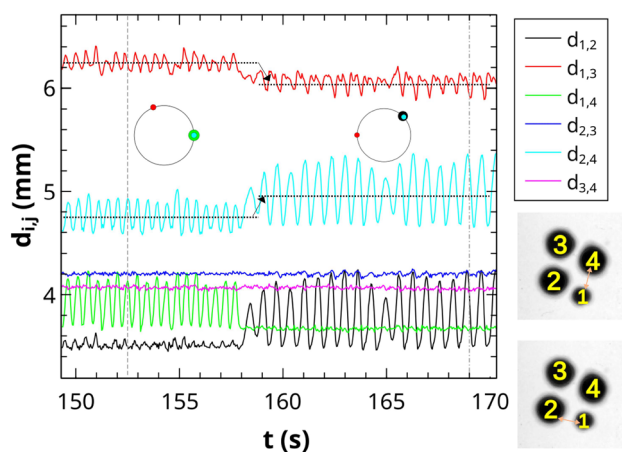

Fig. 10 Dynamics of one small and three big motors: distance between beads i and j ($d_{i,j}$) as a function of time. Phases of oscillation at t = 152.5 s indicated by vertical dashed line shown in the inset in a small circle along with the corresponding top view of the beads (field view: 12 mm × 12 mm) and at t = 169.0 s indicated by vertical dashed dotted line. The orange arrows depict the oscillatory motion between beads.
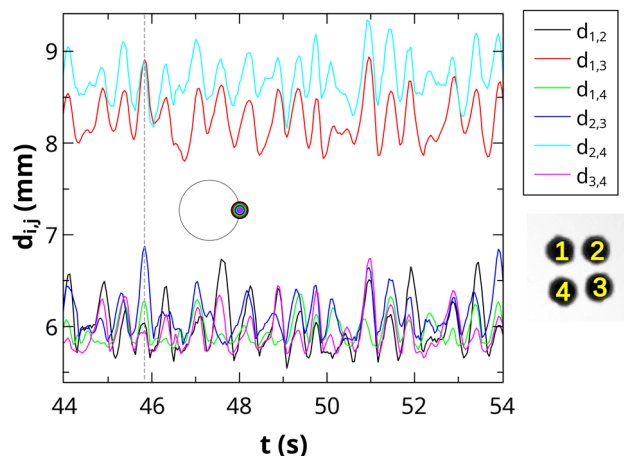

Fig. 11 Dynamics of four big motors: distance between beads i and j ($d_{i,j}$) as a function of time. Phases of oscillation at t = 45.8 s indicated by vertical dashed line shown in the inset in a small circle along with the corresponding top view of the beads (field view: 18 mm × 18 mm).

The horizontal dotted lines passing through the centers of these oscillations indicate that the beads progressively move farther apart.

This change occurs simultaneously with the activity of the diagonally positioned unequal-sized beads (1 and 3), where the mean value of $d_{1,3}$ decreases. Such variations in separation are expected to affect the capillary attraction: for beads 2 and 4, the attraction weakens, whereas for beads 1 and 3, it strengthens. We expect these variations to cause the oscillations of the smaller bead (1), relative to the larger beads, to transition to a new state. The corresponding phase evolution is shown in Fig. S12 in SI, which highlights the coexistence of synchronized and unsynchronized distance variations that is characterized with a decrease in the maximum cross-correlations (see Fig. S7 in SI).

Finally, we investigated the collective behavior of nearly identical, larger (4.53 mm diameter) chitosan-based self-propelled motors. As shown in Fig. 11, the distances between all beads vary approximately in phase, indicating a breathing-type motion. During this breathing motion, characterized by the synchronous "open–close" movement of the beads, the separations $d_{i,j}$ fluctuate significantly, leading to irregular oscillatory dynamics of the system with smaller maximum cross-correlations (see Fig. S8 in SI).

4 Conclusions

The collective behavior of three to four active surfers, in the form of chitosan beads, has been investigated on an aqueous solution. The rich dynamics of their motion at the air–liquid interface is governed by their size distribution. The interplay between capillary attraction and Marangoni-driven repulsion, when they have similar magnitudes, can lead to oscillatory motion between two beads. When more surfers are brought together, either by their self-propulsion or by external stimuli, the oscillators can interact *via* modifying the ethanol concentration, and hence, the surface tension of the liquid, driving the repulsion, and *via* depressing the liquid surface needed for

capillary attraction. Both mechanisms are size-dependent and provide an effective coupling, giving rise to diverse synchronization states. Assemblies of three or four beads of equal size generally form symmetric configurations that exhibit breathing motion, where each bead oscillates back and forth relative to the center of mass in phase. In rare cases, when the assembly forms at a later stage with weaker Marangoni expulsion, the beads lack sufficient motility to regenerate the symmetric configuration and instead become trapped in an asymmetric state, although some oscillatory activity persists.

Introducing size asymmetry profoundly alters the dynamical states: pairs of smaller beads display oscillations, while larger beads act as stabilizing anchors, leading to partial synchrony or dynamical frustration. In our experiments, the system showed sensitivity to initial conditions, attributed to asymmetry at the edges of the beads,[23] the time of assembly, and the relative positioning of the beads within the cluster. These factors led to qualitatively different cluster movements (translational or rotational) and modes of collective motion. They also influenced the local environment, giving rise to distinct dynamical regimes, including switching between synchronized states and the coexistence of synchronized and unsynchronized states. This work provides insights into how tunable attractive–repulsive interactions serve as a model platform for exploring routes to synchrony in active systems, with implications for designing controlled collective behaviors in artificial self-propelled particles.

Author contributions

BG: investigation, visualization, PK: conceptualization, validation, writing – original draft, DH: methodology, software, resources, AT: conceptualization, supervision, resources, validation, writing – original draft. All authors reviewed and edited the manuscript.

Conflicts of interest

There are no conflicts to declare.

Data availability

The data supporting this article have been included in the main text and in the supplementary information (SI). Supplementary information: size effects on capillary attraction, quantification of synchronization by cross-correlation with heat maps, temporal evolution of phases for several cases, trajectories for scenarios with two small and two big beads varying initial conditions, several videos of collective behavior of chitosan beads, data related to the figures in a zip file. See DOI: **https://doi.org/10.1039/d5sm00857c**.

Acknowledgements

References

1 M. C. Marchetti, J.-F. Joanny, S. Ramaswamy, T. B. Liverpool, J. Prost, M. Rao and R. A. Simha, Hydrodynamics of soft active matter, *Rev. Mod. Phys.*, 2013, **85**, 1143–1189.

2 C. Chen, S. Liu, X.-Q. Shi, H. Chaté and Y. Wu, Weak synchronization and large-scale collective oscillation in dense bacterial suspensions, *Nature*, 2017, **542**, 210–214.

3 J. Krause, G. D. Ruxton and S. Krause, Swarm intelligence in animals and humans, *Trends Ecol. Evol.*, 2010, **25**, 28–34.

4 V. Pimienta and C. Antoine, Self-propulsion on liquid surfaces, *Curr. Opin. Colloid Interface Sci.*, 2014, **19**, 290–299.

5 J. Chen, C. Yang and Z.-S. Mao, The interphase mass transfer in liquid-liquid systems with Marangoni effect, *Eur. Phys. J.-Spec. Top.*, 2015, **224**, 389–399.

6 S. Nakata, M. Nomura, H. Yamamoto, S. Izumi, N. J. Suematsu, Y. Ikura and T. Amemiya, Periodic Oscillatory Motion of a Self-Propelled Motor Driven by Decomposition of H_2O_2 by Catalase, *Angew. Chem.*, 2017, **129**, 879–882.

7 Q. Wang, P. Knoll and O. Steinbock, Self-propelled chemical garden tubes, *J. Phys. Chem. B*, 2021, **125**, 13908–13915.

8 J. L. Moran and J. D. Posner, Phoretic self-propulsion, *Annu. Rev. Fluid Mech.*, 2017, **49**, 511–540.

9 S. Nakata and K. Matsuo, Characteristic self-motion of a camphor boat sensitive to ester vapor, *Langmuir*, 2005, **21**, 982–984.

10 Y. Xu, N. Takayama, H. Er and S. Nakata, Oscillatory motion of a camphor object on a surfactant solution, *J. Phys. Chem. B*, 2021, **125**, 1674–1679.

11 T. Fujino, M. Matsuo, V. Pimienta and S. Nakata, Oscillatory Motion of an Organic Droplet Reflecting a Reaction Scheme, *J. Phys. Chem. Lett.*, 2023, **14**, 9279–9284.

12 H. Er, Y. Bai, M. Matsuo and S. Nakata, Oscillatory Motion of a Camphor Disk on a Water Phase with an Ionic Liquid Sensitive to Transition Metal Ions, *J. Phys. Chem. B*, 2025, **129**, 592–597.

13 L. R. Holstein, N. J. Suematsu, M. Takeuchi, K. Harano, T. Banno and A. Takai, Reduction-Induced Self-Propelled Oscillatory Motion of Perylenediimides on Water, *Angew. Chem.*, 2024, **63**, e202410671.

14 S. Sur, H. Masoud and J. P. Rothstein, Translational and rotational motion of disk-shaped Marangoni surfers, *Phys. Fluids*, 2019, **31**, 102101.

15 M. Leoni, M. Paoluzzi, S. Eldeen, A. Estrada, L. Nguyen, M. Alexandrescu, K. Sherb and W. W. Ahmed, Surfing and crawling macroscopic active particles under strong confinement: Inertial dynamics, *Phys. Rev. Res.*, 2020, **2**, 043299.

16 I. Tiwari, P. Parmananda and R. Chelakkot, Periodic oscillations in a string of camphor infused disks, *Soft Matter*, 2020, **16**, 10334–10344.

17 L. Keiser, H. Bense, P. Colinet, J. Bico and E. Reyssat, Marangoni bursting: evaporation-induced emulsification

of binary mixtures on a liquid layer, *Phys. Rev. Lett.*, 2017, **118**, 074504.

18 K. Nagai, Y. Sumino, H. Kitahata and K. Yoshikawa, Mode selection in the spontaneous motion of an alcohol droplet, *Phys. Rev. E: Stat., Nonlinear, Soft Matter Phys.*, 2005, **71**, 065301.

19 J. M. P. Gutierrez, T. Hinkley, J. W. Taylor, K. Yanev and L. Cronin, Evolution of oil droplets in a chemorobotic platform, *Nat. Commun.*, 2014, **5**, 5571.

20 F. Wodlei, J. Sebilleau, J. Magnaudet and V. Pimienta, Marangoni-driven flower-like patterning of an evaporating drop spreading on a liquid substrate, *Nat. Commun.*, 2018, **9**, 820.

21 A. A. Khatun, A. Chotalia, K. Das, S. Dixit and P. Parmananda, Surface tension gradient invoked path selection, *Phys. Chem. Chem. Phys.*, 2024, **26**, 25590–25598.

22 S. Dixit, A. Chotalia, S. Shukla, T. Roy and P. Parmananda, Pathway selection by an active droplet, *Soft Matter*, 2023, **19**, 6844–6850.

23 P. Kumar, D. Horváth and Á. Tóth, Sol-gel transition programmed self-propulsion of chitosan hydrogel, *Chaos*, 2022, **32**, 063120.

24 R. Zahorán, P. Kumar, D. Horváth and Á. Tóth, Self-propulsion of a calcium alginate surfer, *Soft Matter*, 2023, **19**, 8033–8039.

25 S. Soh, K. J. Bishop and B. A. Grzybowski, Dynamic self-assembly in ensembles of camphor boats, *J. Phys. Chem. B*, 2008, **112**, 10848–10853.

26 S. Nakata, Y. Doi and H. Kitahata, Synchronized sailing of two camphor boats in polygonal chambers, *J. Phys. Chem. B*, 2005, **109**, 1798–1802.

27 M. I. Kohira, Y. Hayashima, M. Nagayama and S. Nakata, Synchronized self-motion of two camphor boats, *Langmuir*, 2001, **17**, 7124–7129.

28 S. Nakata, K. Kayahara, M. Kuze, E. Ginder, M. Nagayama and H. Nishimori, Synchronization of self-propelled soft pendulums, *Soft Matter*, 2018, **14**, 3791–3798.

29 J. Sharma, I. Tiwari, D. Das, P. Parmananda and V. Pimienta, Rotational synchronization of camphor ribbons in different geometries, *Phys. Rev. E*, 2020, **101**, 052202.

30 J. Sharma, I. Tiwari, D. Das and P. Parmananda, Chimera-like states in a minimal network of active camphor ribbons, *Phys. Rev. E*, 2021, **103**, 012214.

31 T. Roy, S. S. Chaurasia, J.-M. Cruz, V. Pimienta and P. Parmananda, Modes of synchrony in self-propelled pentanol drops, *Soft Matter*, 2022, **18**, 1688–1695.

32 P. Kumar, Q. Wang, D. Horváth, Á. Tóth and O. Steinbock, Collective motion of self-propelled chemical garden tubes, *Soft Matter*, 2022, **18**, 4389–4395.

33 P. J. de Visser, M. Neeleman, P. F. Dankloff, M. T. Derks and P. A. Korevaar, Positional Information-Based Organization of Surfactant Droplet Swarms Emerging from Competition Between Local and Global Marangoni Effects, *Small*, 2024, **20**, 2403720.

34 P. Singh and P. A. Korevaar, Predator-Prey Behavior of Droplets Propelling Through Self-Generated Channels in Crystalline Surfactant Layers, *Angew. Chem.*, 2025, e202502352.

35 P. J. de Visser, D. Karagrigoriou, A.-D. C. Nguindjel and P. A. Korevaar, Quorum Sensing in Emulsion Droplet Swarms Driven by a Surfactant Competition System, *Adv. Sci.*, 2024, **11**, 2307919.

36 D. Liu, A. Mahmood, D. Weng and J. Wang, Life-Like Motion of Oil Drops at the Air-Liquid Interface, *Langmuir*, 2019, **35**, 16146–16152.

37 Q. He, D. Liu, W. Huang and J. Wang, Interactions of oil drops induced by the lateral capillary force and surface tension gradients, *Langmuir*, 2019, **35**, 14967–14973.

38 G. Kokot, D. Piet, G. M. Whitesides, I. S. Aranson and A. Snezhko, Emergence of reconfigurable wires and spinners via dynamic self-assembly, *Sci. Rep.*, 2015, **5**, 9528.

39 J. Čejková, K. Schwarzenberger, K. Eckert and S. Tanaka, Dancing performance of organic droplets in aqueous surfactant solutions, *Colloids Surf., A*, 2019, **566**, 141–147.

40 P. Kumar, D. Horváth and Á. Tóth, Self-assembly to synchrony of active gels, *Soft Matter*, 2023, **19**, 4137–4143.

41 T. Roy, S. S. Chaurasia and P. Parmananda, Phase-flip transition in volume-mismatched pairs of coupled 1-pentanol drops, *Phys. Rev. E*, 2022, **106**, 034614.